Series expansions for three-dimensional QED

C. J. Hamer,* J. Oitmaa,† and Zheng Weihong‡
School of Physics, The University of New South Wales, Sydney, NSW 2052, Australia
(Received 18 September 1997; published 23 January 1998)

Strong-coupling series expansions are calculated for the Hamiltonian version of compact lattice electrodynamics in (2+1) dimensions, with 4-component fermions. Series are calculated for the ground-state energy per site, the chiral condensate, and the masses of ''glueball'' and positronium states. Comparisons are made with results obtained by other techniques. [S0556-2821(98)00906-0]

PACS number(s): 11.15.Ha, 12.38.Gc

I. INTRODUCTION

Quantum electrodynamics in 2+1 dimensions (QED_3) has generated considerable interest over recent years. The model is super-renormalizable, but shares a number of important features with quantum chromodynamics (QCD) in 3+1 dimensions: it is believed to be confining at large distances (in the quenched approximation, at least), while in the massless fermion limit it displays a chiral-like symmetry which is spontaneously broken [1,2]. It is thus an ideal laboratory for testing nonperturbative methods of analysis. Versions of the model may also be relevant to theories of the new high-T_c superconductors [3]. The version with two-component massless fermions generates a dynamical mass for the photon through a Chern-Simons term [4]. This complication can be avoided in the four-component version [1,5], where ''chiral'' symmetry is broken in the normal Goldstone fashion, leading to a doublet of massless Goldstone bosons analogous to the pion in QCD. For the four-component model with N_f flavors of massless fermions, there has been a debate running for some time whether chiral symmetry is broken for all values N_f [1,2,6] or whether there is a critical value $N_c \simeq 3.5$ above which no spontaneous symmetry-breaking takes place [7–10]. We shall have nothing to say about this question.

The four-component version has been studied by several different techniques, but we remain far from a complete understanding of the model. Euclidean lattice Monte Carlo simulations have been performed by several groups [7,11,12]. A number of authors [2,6,9,13,14] have used Schwinger-Dyson techniques to study the chiral symmetry breaking, and Allen and Burden [15] have also produced estimates of the bound-state meson spectrum at finite fermion masses. The Hamiltonian lattice version has been studied by means of strong-coupling expansions [16] and a loop expansion technique [17]. A light-front approach has also been discussed [18,19]; and the nonrelativistic limit has been analyzed in some detail [15,19–21].

Here we treat the Hamiltonian lattice model by using linked-cluster techniques [22] to generate further strong-coupling series, thus extending the previous results of Burden and Hamer [16] (hereafter referred to as I). It is well-known that Euclidean Monte Carlo techniques are difficult and expensive to apply to models with dynamical fermions, and so it seems worthwhile to see if other techniques such as strong-coupling expansions can give useful information in such cases. A previous analysis of the Schwinger model [23] did indeed show that strong-coupling series approximants can converge well into the weak coupling region. While not quite as accurate as the exact finite-lattice technique, the series approach did give quantitative estimates of the lowest bound-state mass in the continuum limit, at about the 5–10 % level of accuracy.

The paper begins with an outline of the lattice formulation of the model in Sec. II, followed by a brief summary of the methods of calculation in Sec. III. Our results are presented in Sec. IV, discussing the ground-state energy, the chiral condensate, the ''glueball'' masses, and the spectrum of the bound-state mesons as a function of the bare fermion mass. Our conclusions are summarized in Sec. V.

II. FORMALISM

A. Continuum formulation

The continuum Lagrangian density takes the standard form

$$\mathcal{L} = -\frac{1}{4} F_{\mu\nu} F^{\mu\nu} + \overline{\psi}(i\not{\partial} - e\not{A} - m)\psi \tag{1}$$

where

$$F_{\mu\nu} = \partial_\mu A_\nu - \partial_\nu A_\mu \tag{2}$$

and the Lorentz indices $\mu, \nu = 0$, 1 or 2. The electric coupling e in (2+1) dimensions has the dimensions of $(\text{mass})^{1/2}$. Choosing the timelike axial gauge

$$A_0 = 0 \tag{3}$$

the Hamiltonian is found to be

$$H = \int d^2x \left\{ -i\overline{\psi}(\vec{\gamma}\cdot\vec{\nabla} + ie\vec{\not{A}})\psi + m\overline{\psi}\psi + \frac{1}{2}(\vec{E}^2 + B^2) \right\} \tag{4}$$

where

$$E^i = F^{i0} = -\dot{A}^i \tag{5a}$$

*Email address: c.hamer@unsw.edu.au
†Email address: otja@newt.phys.unsw.edu.au
‡Email address: w.zheng@unsw.edu.au

and

$$B=\partial_1 A^2-\partial_2 A^1. \tag{5b}$$

Note that the magnetic field B has only one component in (2+1)D. Here ψ is taken as a single four-component Dirac spinor [2], and γ_0, γ_1, γ_2 are 4×4 Dirac matrices, for which we shall use the Dirac representation where necessary:

$$\gamma_0=\begin{pmatrix}\sigma_3 & 0\\ 0 & -\sigma_3\end{pmatrix},\quad \gamma_1=i\begin{pmatrix}\sigma_1 & 0\\ 0 & -\sigma_1\end{pmatrix},$$

$$\gamma_2=i\begin{pmatrix}\sigma_2 & 0\\ 0 & -\sigma_2\end{pmatrix}. \tag{6}$$

In the zero-mass limit, the Hamiltonian (4) possesses a global U(2) ''chiral'' symmetry [2], whose Lie algebra is spanned by the matrices

$$I,\ \gamma_4=\begin{pmatrix}0 & I\\ I & 0\end{pmatrix},\quad \gamma_5=i\begin{pmatrix}0 & -I\\ I & 0\end{pmatrix}, \tag{7}$$

and $\gamma_{45}=-i\gamma_4\gamma_5$. This symmetry is expected to be spontaneously broken [2], which should be manifested by a nonzero value of the chiral condensate $\langle\overline{\psi}\psi\rangle_0$.

At large fermion masses, a nonrelativistic analysis can be carried out [19–21]. Cornwall and Tiktopoulos and Sen [20] showed that if the divergences were regulated by giving a mass ν to the photon, then at one-loop order the renormalized self-mass of the fermion is

$$m_R=m+\frac{e^2}{4\pi}\ln\left(\frac{2m}{\nu}\right) \tag{8}$$

while the potential due to one-photon exchange between the electron and positron is

$$V(r)=-e^2\int\frac{d^2k}{(2\pi)^2}\,\frac{e^{i\vec{k}\cdot\vec{r}}}{\vec{k}^2+\nu^2}=\frac{e^2}{2\pi}\left(\gamma+\ln\frac{\nu r}{2}\right)+O(\nu^2r^2) \tag{9}$$

where γ is Euler's constant. Both quantities show logarithmic divergences, but these divergences cancel in the Schrödinger equation for the positronium bound states

$$E\Psi(\vec{r})=\left[-\frac{1}{m}\vec{\nabla}_r^2+2(m_R-m)+V(r)\right]\psi(\vec{r})$$

$$=\left[-\frac{1}{m}\vec{\nabla}_r^2+\frac{e^2}{2\pi}(\gamma+\ln mr)\right]\psi(\vec{r}). \tag{10}$$

Numerical solutions of this equation [19–21] give the ''binding energies'' of the lowest positronium states as

$$E_0^0=\frac{e^2}{2\pi}\left(1.7968-\frac{1}{2}\ln\left(\frac{2g^2}{m\pi}\right)\right) \tag{11a}$$

$$E_1^0=\frac{e^2}{2\pi}\left(2.9323-\frac{1}{2}\ln\left(\frac{2g^2}{m\pi}\right)\right) \tag{11b}$$

for angular momentum $l=0$, and

$$E_0^1=\frac{e^2}{2\pi}\left(2.6566-\frac{1}{2}\ln\left(\frac{2g^2}{m\pi}\right)\right) \tag{12}$$

for $l=1$. At leading order the binding energies are independent of ''spin,'' so that each of these energy levels should be fourfold degenerate in the four-component fermion model.

B. Lattice formulation

A ''staggered'' Hamiltonian lattice formulation of this model has been discussed in reference I. The four components of the continuum fermion field fit naturally onto the four sites of a 2×2 unit cell on the 2-dimensional spatial lattice, leading to a lattice Hamiltonian as follows:

$$H=\frac{g^2}{2a}W \tag{13}$$

where

$$W=W_0+yW_1+y^2W_2 \tag{14}$$

and[1]

$$W_0=W_e+W_\mu=\sum_l E_l^2+\mu\sum_{\vec{r}}(-1)^{r_1+r_2+1}\chi^\dagger(\vec{r})\chi(\vec{r}) \tag{15a}$$

$$W_1=\sum_{\vec{r},i}\eta_i(\vec{r})[\chi^\dagger(\vec{r})U_i(\vec{r})\chi(\vec{r}+\hat{i})+\text{H.c.}] \tag{15b}$$

$$W_2=-\sum_p(U_p+U_p^\dagger). \tag{15c}$$

Here $\vec{r}=(r_1,r_2)$ labels the sites, l the links, p the plaquettes and $i=1,2$ the directions on a square two-dimensional spatial lattice with spacing a. The dimensionless coupling g and mass parameter μ are defined in terms of their continuum counterparts e and m by

$$g^2=e^2a\ \text{ and }\ \mu=\frac{2am}{g^2}=\frac{2m}{e^2} \tag{16}$$

while $y=1/g^2$, and $\eta_1(\vec{r})=(-1)^{r_2+1}$, $\eta_2(\vec{r})=1$. The term W_e is the electric field term, W_μ is the fermion mass term, W_1 is the fermion kinetic energy, and W_2 is the magnetic field energy, involving the usual plaquette operator U_p.

The correspondences between the lattice fields and their continuum counterparts are for gauge fields

$$\frac{e}{a}E_l\to E^i(\vec{x}) \tag{17a}$$

$$A_l\to A^i(\vec{x}) \tag{17b}$$

where the link operator

[1]The fermion mass term given in reference I had the wrong sign. As it turns out, that did not affect the results for the quantities they calculated.

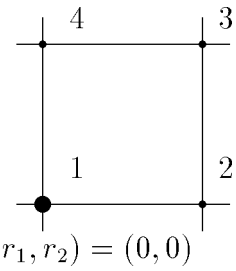

FIG. 1. Assignment of spinor components to sites of the 2×2 unit cell.

$$U_l = \exp[iaeA_l(\vec{r})] \tag{18}$$

while for the fermion field components

$$\frac{1}{2\sqrt{2}a}\begin{bmatrix} 0 & -i & 0 & 1 \\ 1 & 0 & -i & 0 \\ -i & 0 & 1 & 0 \\ 0 & 1 & 0 & -i \end{bmatrix}\begin{bmatrix} \xi_1 \\ \xi_2 \\ \xi_3 \\ \xi_4 \end{bmatrix} \rightarrow \begin{bmatrix} \psi_1 \\ \psi_2 \\ \psi_3 \\ \psi_4 \end{bmatrix} \tag{19}$$

where [24]

$$\xi(\vec{r}) = i^{r_1+r_2}\chi(\vec{r}) \tag{20}$$

and the components $1,\ldots,4$ are assigned to sites of the 2×2 unit cell as shown in Fig. 1.

The commutation relations between the lattice fields are

$$[E_l, U_{l'}] = U_l\delta_{ll'} \tag{21a}$$

$$[E_l, U_{l'}^\dagger] = -U_l^\dagger\delta_{ll'} \tag{21b}$$

$$\{\chi^\dagger(\vec{r}), \chi(\vec{r}')\} = \delta_{\vec{r},\vec{r}'} \tag{21c}$$

$$[E_l, \chi(\vec{r})] = [E_l, \chi^\dagger(\vec{r})] = [U_l, \chi(\vec{r})] = [U_l, \chi^\dagger(\vec{r})] = 0. \tag{21d}$$

With these correspondences, it can be shown [16] that the lattice Hamiltonian (13) reduces to the continuum Hamiltonian (4) in the naive continuum limit $a\rightarrow0$.

The introduction of the lattice breaks the U(2) ''chiral'' symmetry down to a discrete symmetry generated by shifts of one lattice spacing [16]. A unit shift in either the x or y direction leaves the kinetic term in the Hamiltonian (13) invariant, but alters the sign of the mass term. The corresponding continuum field transformations, from (19), are

$$\psi \rightarrow e^{i(\pi/2)\gamma_4}\psi \tag{22a}$$

or

$$\psi \rightarrow e^{i(\pi/2)\gamma_5}\psi \tag{22b}$$

respectively.

C. The strong-coupling limit

The Hamiltonian (13) acts on a Fock space spanned by the usual strong-coupling basis [25]. With each link is associated an integer electric flux n_l such that $E_l|n_l\rangle = n_l|n_l\rangle$. The operators U_l and $U_l^\dagger$ increase and decrease the flux on link l by one unit, respectively. Each site of the lattice can be in one of two fermionic states $|+\rangle$ or $|-\rangle$ obeying

$$\chi^\dagger|-\rangle = |+\rangle, \quad \chi^\dagger|+\rangle = 0 \tag{23a}$$

$$\chi|-\rangle = 0, \quad \chi|+\rangle = |-\rangle. \tag{23b}$$

Consider first the massless theory, $\mu=0$. In the strong-coupling limit, the variable $y=0$ and the Hamiltonian W reduces to W_e. The ground state is then highly degenerate, having flux $n_l=0$ on each link, but with the fermionic state entirely arbitrary. This degeneracy is broken at the next order by the kinetic term W_1, leaving only two degenerate states $|A\rangle$ and $|B\rangle$ whose fermionic content is

$$|A\rangle = \begin{cases} |+\rangle, & \text{on odd sites;} \\ |-\rangle, & \text{on even sites} \end{cases} \tag{24}$$

and

$$|B\rangle = \begin{cases} |-\rangle, & \text{on odd sites;} \\ |+\rangle, & \text{on even sites.} \end{cases} \tag{25}$$

The chiral shifts of Eqs. (22a), (22b) map these two states into each other. When the mass term W_μ is included, chiral symmetry is explicitly broken and state $|B\rangle$ is favored energetically. We thus take $|B\rangle$ as the unperturbed strong-coupling ground state for both the massive and massless cases, and interpret this as the state with no fermion excitations present.

An excitation on an odd or even site creates a positively or negatively charged fermion respectively, i.e. a positron or electron. The first-order perturbation W_1 creates or destroys an electron-positron pair on neighboring sites, joined by a link of flux. The second-order perturbation term W_2 creates or destroys a plaquette of flux. Gauge invariance ensures that for any state obtained from the unperturbed vacuum by application of the operators W_1 and W_2, the net flux from any site is equal to the charge of the fermion at that site, i.e., Gauss' law is obeyed.

D. Positronium states

This theory is expected to display confinement [20], and the only fermionic states with finite energy are expected to be electrically neutral ''positronium'' bound states. In the strong-coupling limit, the lowest energy positronium states consist of an electron-positron pair on neighboring sites, connected by a link of unit flux. There are eight translationally-invariant states of this type, corresponding to the eight links in the unit cell, and we need to identify the linear combinations of these states which correspond to eigenstates of the lattice symmetry operators. The corresponding procedure for meson states in four-dimensional Euclidean lattice QCD has been discussed by Golterman [26].

The symmetry group of the lattice Hamiltonian (13) is composed of the following elements:

1. Even translations

$$\chi(\vec{r}) \rightarrow \chi(\vec{r}+2\hat{i}), \quad U_j(\vec{r}) \rightarrow U_j(\vec{r}+2\hat{i}). \tag{26}$$

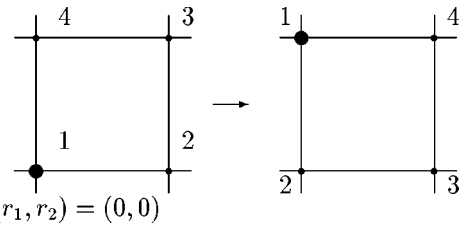

FIG. 2. A square lattice rotation by $\pi/2$. Point 1 is assumed fixed.

This corresponds to spatial translational invariance in the continuum model.

2. Odd translations

$$\chi(\vec{r}) \to \chi(\vec{r}+\hat{1}), \quad U_i(\vec{r}) \to U_i(\vec{r}+\hat{1}) \tag{27a}$$

or

$$\chi(\vec{r}) \to (-1)^{r_1}\chi(\vec{r}+\hat{2}), \quad U_i(\vec{r}) \to U_i(\vec{r}+\hat{2}). \tag{27b}$$

These are the discrete lattice versions of ''chiral'' symmetry corresponding to Eqs. (22a),(22b). The massless Hamiltonian is symmetric under these transformations, but not the massive one.

3. Diagonal shift D

A combination of a shift by one site in the x direction and one site in the y direction gives a diagonal shift

$$\chi(\vec{r}) \to (-1)^{r_1}\chi(\vec{r}+\hat{1}+\hat{2}), \quad U_i(\vec{r}) \to U_i(\vec{r}+\hat{1}+\hat{2}). \tag{28}$$

This corresponds to a discrete γ_{45} rotation in the continuum fields

$$\psi \to i\gamma_{45}\psi. \tag{29}$$

This remains a symmetry of the massive Hamiltonian also.

4. Square lattice rotations, R

Let R denote a lattice rotation by $\pi/2$ about a perpendicular axis, as shown by Fig. 2:

$$\chi(\vec{r}) \to R(\vec{r}\,')\chi(\vec{r}\,') \tag{30a}$$

$$U_2(\vec{r}) \to U_1(\vec{r}\,') \tag{30b}$$

$$U_1(\vec{r}) \to U_2^\dagger(\vec{r}\,'-\hat{2}) \tag{30c}$$

where

$$r_1' = r_2, \quad r_2' = -r_1 \tag{31}$$

and

$$R(r_1,r_2) = \frac{1}{2}[(-1)^{r_1} + (-1)^{r_2} + (-1)^{r_1+r_2} - 1]. \tag{32}$$

Repeated rotations generate the rotational symmetry group of a square, with 4 elements. It corresponds to rotation in both space and ''spin'' in the continuum model.

5. ''Axial parity'' inversion, A

The ''axial parity'' inversion is discussed by Burden and Allen [13,15]. In the continuum, it corresponds to the operations:

$$\psi(x) \to \psi'(x') = A\psi(x), \overline{\psi}(x) \to \overline{\psi}'(x') = \overline{\psi}(x)A^{-1} \tag{33}$$

and the vector field transforms as

$$\vec{A}(x) \to \vec{A}'(x') = -\vec{A}(x) \tag{34}$$

where $x' = (x^0, -x^1, -x^2)$. A suitable representation for the fermion operator A is the matrix $i\gamma_0$.

On the lattice, this is simply

$$\chi(\vec{r}) \to \chi(-\vec{r}) \tag{35a}$$

$$U_i(\vec{r}) \to U_i^\dagger(-\vec{r}-\hat{i}) \tag{35b}$$

which is equivalent to R^2, a rotation by Π in 2+1 dimensions.

6. Reflection, Π

A reflection in the y axis corresponds to

$$\chi(\vec{r}) \to \chi(\vec{r}\,') \tag{36a}$$

$$U_1(\vec{r}) \to U_1^\dagger(\vec{r}\,'-\hat{1}) \tag{36b}$$

$$U_2(\vec{r}) \to U_2(\vec{r}\,') \tag{36c}$$

where

$$r_1' = -r_1, \quad r_2' = r_2. \tag{37}$$

7. Charge conjugation, C

The charge conjugation operation is also discussed by Burden and Allen [13,15]. In the continuum, it corresponds to the operators:

$$\psi(x) \to \psi'(x) = C\overline{\psi}^T(x), \quad \overline{\psi}(x) \to \overline{\psi}'(x) = -\psi^T(x)C^\dagger \tag{38}$$

and

$$A^\mu(x) \to A^{\mu\prime}(x) = -A^\mu(x). \tag{39}$$

The fermion operator can be represented, up to an arbitrary phase, by the matrix γ_2. The translation to lattice variables is slightly involved, and is best handled in terms of the fields ξ_i defined in Eqs. (19), (20). We shall not go into further details here.

The translationally invariant positronium eigenstates can be classified in terms of their eigenvalues under these symmetry operations. The group of square rotations is $\mathcal{C}_4$, the cyclic group of 4 elements. It has 4 irreducible representations, each with dimension 1. The allowed eigenvalues of R simply consist of the 4th roots of unity (i.e. powers of $\epsilon \equiv e^{-2\pi i/4}$). The shift D, reflection Π and axial parity A each generate 2-element groups, with eigenvalues ± 1 for the positronium states with translational symmetry.

TABLE I. Link excitations on the unit cell corresponding to positronium states in the strong-coupling limit, with sites labelled according to Fig. 3.

Link state	Operator equivalent
$\|1\rangle$	$\chi^\dagger(2)U_1^\dagger(1)\chi(1)$
$\|2\rangle$	$\chi^\dagger(2)U_1(2)\chi(5)$
$\|3\rangle$	$\chi^\dagger(4)U_2^\dagger(1)\chi(1)$
$\|4\rangle$	$\chi^\dagger(4)U_2(4)\chi(8)$
$\|5\rangle$	$\chi^\dagger(4)U_1(4)\chi(3)$
$\|6\rangle$	$\chi^\dagger(6)U_1^\dagger(3)\chi(3)$
$\|7\rangle$	$\chi^\dagger(2)U_2(2)\chi(3)$
$\|8\rangle$	$\chi^\dagger(7)U_2^\dagger(3)\chi(3)$

In the strong-coupling limit, the ''link excitations'' on the unit cell corresponding to the lowest energy positronium states consist of the eight states listed in Table I, numbered according to Fig. 3. These states transform into each other under the action of the symmetry operators. By taking linear combinations of these states, one can form eigenstates $|\psi_1\rangle, \ldots, |\psi_8\rangle$ of the lattice symmetry operators, as listed in Table II. Note that the states with rotation eigenvalue $R=\epsilon=-i$ or $R=\epsilon^3=-i$ cannot simultaneously be eigenstates of Π, because a reflection converts $R=i$ to $R=-i$, and vice versa. We have chosen to list states $|\psi_5\rangle$ to $|\psi_8\rangle$ which correspond to eigenstates of Π, and are thus symmetric or antisymmetric combinations of the states with $R=\pm i$. Similarly, we have chosen to list states $|\psi_2\rangle$ and $|\psi_4\rangle$ which are eigenstates of C, rather than R. All eight states are degenerate in energy in the strong-coupling limit $y\to 0$. The fact that the Hamiltonian is symmetric under both rotations and reflections implies that the pair $|\psi_5\rangle$ and $|\psi_6\rangle$ will remain degenerate at all couplings, and likewise the pair $|\psi_7\rangle$ and $|\psi_8\rangle$. The combination of rotation and charge conjugation symmetry implies that the pair $|\psi_2\rangle$ and $|\psi_4\rangle$ will also remain degenerate.

In the ''naive continuum limit'' $a\to 0$, when $U_l\to 1+ieaA_l$, one finds that the quartet of states $|\psi_5\rangle$ to $|\psi_8\rangle$ transcribe to simple combinations of quark and antiquark fields on the lattice, and correspond to ''vector'' states in the language of Burden and Allen [13,15], with $J^{AC}=1^{--}$, where J is the ''total angular momentum.'' The states $|\psi_1\rangle$ to $|\psi_4\rangle$, on the other hand, contain an admixture of gauge fields in the naive continuum limit, and have no direct counterparts in the catalogue of quark-antiquark states discussed by Burden and Allen. The state $|\psi_1\rangle$ is a scalar state, having the same quantum numbers as the vacuum.

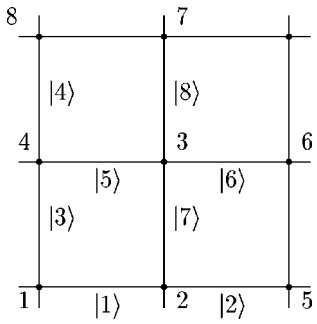

FIG. 3. Numbering of sites and ''link'' states on the unit cell.

E. Weak-coupling expansion

Some useful information on the ground-state properties, at least, can be gained by performing a ''weak-coupling'' expansion for the lattice system as $y\to\infty$. For the present model, this exercise was carried out in reference I.

The ground-state energy per site has an asymptotic expansion in the weak-coupling limit:

$$\omega_0 \sim -2y^2 + 1.9162y - \frac{4y}{\pi^2}\int_0^{\pi/2} dq_1 \int_0^{\pi/2} dq_2 \left[\cos^2 q_1 + \cos^2 q_2 + \frac{\mu^2}{4y^2}\right]^{1/2} + O(1) \quad \text{as} \quad y\to\infty \tag{40}$$

where the integral arises from a sum over the fermionic degrees of freedom. At very large y one finds

TABLE II. Linear combinations of the link states forming eigenstates of the lattice symmetry group ($|\psi_j\rangle = a_l^j|i\rangle$), and their symmetry eigenvalues.

State:	$\|\psi_1\rangle$	$\|\psi_2\rangle$	$\|\psi_3\rangle$	$\|\psi_4\rangle$	$\|\psi_5\rangle$	$\|\psi_6\rangle$	$\|\psi_7\rangle$	$\|\psi_8\rangle$
				Amplitudes of the link states				
a_1	1	1	1	0	1	0	1	0
a_2	1	1	1	0	−1	0	−1	0
a_3	−1	0	1	1	0	1	0	1
a_4	−1	0	1	1	0	−1	0	−1
a_5	−1	1	−1	0	1	0	−1	0
a_6	−1	1	−1	0	−1	0	1	0
a_7	−1	0	1	−1	0	−1	0	1
a_8	−1	0	1	−1	0	1	0	−1
				Eigenvalues				
R	+1	−	−1	−	−	−	−	−
D	+1	−1	+1	−1	+1	+1	−1	−1
Π	+1	+1	+1	+1	−1	+1	−1	+1
C	+1	+1	+1	−1	−1	−1	−1	−1
A	+1	+1	+1	+1	−1	−1	−1	−1

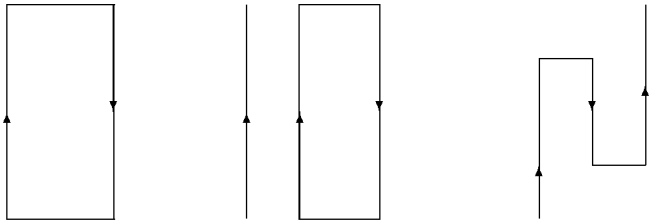

FIG. 4. Lattice perturbation theory diagrams at second order involving excitation of an (e^+e^-) pair. The associated gauge field excitations are not shown. Horizontal lines represent the action of ''link'' excitation operators from W_1; vertical lines represent the resulting fermion excitations.

$$\omega_0 \sim -2y^2 + 0.9581y + O(1) \quad \text{as} \quad y \to \infty \tag{41}$$

but for finite y and μ it is more useful to evaluate the integral as it stands.

The ground-state expectation value of the chiral condensate was also calculated [16] as

$$\langle \overline{\psi}\psi \rangle^{\text{lattice}} \sim -\frac{\mu}{\pi^2 y}\int_0^{\pi/2} dq_1 \int_0^{\pi/2} dq_2 \left[\cos^2 q_1 + \cos^2 q_2 + \frac{\mu^2}{4y^2} \right]^{-1/2} + O(y^{-2}) \quad \text{as} \quad y \to \infty \tag{42}$$

where

$$\langle \overline{\psi}\psi \rangle^{\text{lattice}} = \left\langle \psi_0 \left| \frac{1}{N} \sum_{\vec{r}} (-1)^{r_1+r_2+1} \chi^\dagger(\vec{r}) \chi(\vec{r}) \right| \psi_0 \right\rangle \tag{43}$$

$$= \frac{1}{e^4 y^2} \langle \overline{\psi}\psi \rangle^{\text{continuum}} \tag{44}$$

in terms of the continuum chiral condensate. This quantity is given by the Feynman Hellmann theorem as

$$\langle \overline{\psi}\psi \rangle^{\text{lattice}} = \frac{1}{N} \frac{\partial \omega_0}{\partial \mu} \tag{45}$$

where ω_0 is the ground-state eigenvalue of W.

F. Nonrelativistic limit $m/e^2 \to \infty$

When the fermion mass m becomes very large, it should be possible to study the model in a ''quenched'' approximation, where fermion loop diagrams are suppressed. In a staggered lattice formulation such as the present one, the suppression of all fermion loops will lead to the ''static'' limit, in which any fermion excitation is fixed at its initial lattice site, and apart from the mass term the remaining lattice Hamiltonian is simply that of the pure gauge theory.

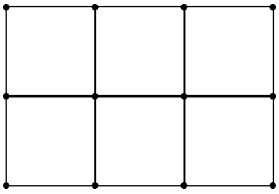

FIG. 5. The last graphs contributing at order y^{22}.

To allow the fermions to move or migrate on the lattice, one has to go to the next order in powers of $1/\mu$, the mass parameter, and allow second-order diagrams involving the excitation of an (e^+e^-) pair on neighboring sites, as shown in Fig. 4. Figure 4(a) represents a loop diagram in the vacuum sector, and 4(b) a similar diagram in the one-fermion sector; Fig. 4(c) illustrates a ''hopping'' diagram, in which an existing fermion hops two lattice sites. This allows fermion migration to take place.

It is useful to define new fermion variables representing the excitations on the strong-coupling ground-state: namely,

$$\phi(\vec{r}) = \begin{cases} \chi^\dagger(\vec{r}), & (r_1+r_2)\text{even}; \\ \chi(\vec{r}), & (r_1+r_2)\text{odd}. \end{cases} \tag{46}$$

so that

$$\phi(\vec{r})|0\rangle = 0 \tag{47}$$

where $|0\rangle = |B\rangle$ is the strong-coupling ground state. The Hamiltonian (14) and link excitations (Table I) are easily translated in terms of the new variables.

In the quenched approximation outlined above, the effective Hamiltonian in the vacuum sector is

$$W^0_{\text{eff}} = -\frac{N}{2}\mu - N\frac{y^2}{\mu} + W_e + y^2 W_2 \tag{48}$$

(where N is the number of sites on the lattice) which is simply the pure gauge field Hamiltonian plus a constant. The first constant term is the negative energy of the ''Dirac sea'' on the lattice, while the second constant term is the contribution of the second-order diagram, Fig. 4(a). More interesting is the effective Hamiltonian in the (e^+e^-) sector, which takes the form

$$W^{e^+e^-}_{\text{eff}} = -\frac{(N-4)}{2}\mu - (N-4)\frac{y^2}{\mu} + W_e + y^2 W_2 + y^2 W_1' \tag{49}$$

where

$$W_1' = \frac{1}{2\mu}\sum_{\vec{r}\ \mathrm{odd}} (-1)^{\phi^\dagger\phi(\vec{r})}\{\phi^\dagger(\vec{r}-\hat{1})U_1^\dagger(\vec{r}-\hat{1})[U_1^\dagger(\vec{r})\phi(\vec{r}+\hat{1})+(-1)^{r_2+1}(U_2(\vec{r}-\hat{2})\phi(\vec{r}-\hat{2})+U_2^\dagger(\vec{r})\phi(\vec{r}+\hat{2}))]$$
$$+\phi^\dagger(\vec{r}-\hat{2})U_2^\dagger(\vec{r}-\hat{2})[U_2(\vec{r})\phi(\vec{r}+\hat{2})+(-1)^{r_2+1}U_1^\dagger(\vec{r})\phi(\vec{r}+\hat{1})]+(-1)^{r_2+1}\phi^\dagger(\vec{r}+\hat{2})U_2(\vec{r})U_1(\vec{r})\phi(\vec{r}+\hat{1})+\mathrm{H.c.}\}$$
$$+\frac{1}{2\mu}\sum_{\vec{r}\ \mathrm{even}} (-1)^{\phi^\dagger\phi(\vec{r})}\{\phi^\dagger(\vec{r}-\hat{1})U_1(\vec{r}-\hat{1})[U_1(\vec{r})\phi(\vec{r}+\hat{1})+(-1)^{r_2+1}(U_2^\dagger(\vec{r}-\hat{2})\phi(\vec{r}-\hat{2})+U_2(\vec{r})\phi(\vec{r}+\hat{2}))]$$
$$+\phi^\dagger(\vec{r}-\hat{2})U_2(\vec{r}-\hat{2})[U_2^\dagger(\vec{r})\phi(\vec{r}+\hat{2})+(-1)^{r_2+1}U_1(\vec{r})\phi(\vec{r}+\hat{1})]+(-1)^{r_2+1}\phi^\dagger(\vec{r}+\hat{2})U_2^\dagger(\vec{r})U_1^\dagger(\vec{r})\phi(\vec{r}+\hat{1})+\mathrm{H.c.}\}. \tag{50}$$

This clumsy expression is merely a constant, plus the pure gauge Hamiltonian, plus ''hopping'' terms for the fermions in the six different paths allowed for a double hop on the staggered lattice. The associated phase factor

$$(-1)^{\phi^\dagger\phi(\vec{r})} \equiv \begin{cases} +1, & \text{if site } \vec{r} \text{ occupied;} \\ -1, & \text{if site } \vec{r} \text{ unoccupied} \end{cases} \tag{51}$$

accounts for the change of sign if the hopping fermion ''passes through'' an occupied site. These hopping terms correspond to the kinetic energy in the nonrelativistic continuum Hamiltonian.

The effective Hamiltonian is more complicated in form than the original lattice Hamiltonian, but does not allow any further fermion excitations, and would therefore be quicker and easier to implement in numerical calculations. We have not attempted any such calculations as yet.

III. METHOD

To calculate the strong-coupling series for the model, we used Nickel's cluster expansion method. The techniques necessary were reviewed in He *et al.* [22], and will not be repeated here. In these calculations, the W_0 in Eq. (14) is taken as the unperturbed Hamiltonian, diagonal in the basis of eigenvectors of E_l, while the W_1 and W_2 in Eq. (14) then act as perturbations.

To generate the series for the ground state energy, we need to generate a list of connected plaquette configurations, together with their lattice constants and embedding constants. Since the first-order perturbation W_1 and second-order perturbation W_2 involve links and plaquettes, respectively, a cluster α will contribute terms $O(y^\alpha)$, where α is given by

$$\alpha \geq 2n_p + n_l \tag{52}$$

where n_p is the number of plaquettes in α, and n_l the number of links not contained in plaquettes. Up to the order y^{22} considered in the current paper, there is only one graph (Fig. 5) which does not obey the above relation, it actually contributes to order y^{22} (due to the combination of W_2 on each plaquette and W_1 in outer links) instead of y^{24} according to Eq. (52). There are a total of 5494 graphs which contribute up to order y^{22} for the ground-state properties.

The calculation of glueball masses involves a list of clusters, both connected and disconnected, with at least one plaquette in each graph. There are 457 graphs which contribute to order y^{10}.

The calculation of meson masses generally involves a list of both connected and disconnected clusters [22]. The eight different links in the unit cell (shown in Fig. 3) are not equivalent in those calculations, which means we cannot identify clusters which are topologically equivalent, or even use rotation or reflection symmetry. Thus the separate clusters proliferate enormously in this case: there are 164142 clusters contributing up to order y^{10}. For the scalar meson mass m_1, the eight different bond types are equivalent, so we only need actually one bond type, and there are only 569 clusters which contribute up to order y^{12}.

IV. RESULTS

A. Ground-state energy

Using the linked-cluster expansion method, series have been calculated for the ground-state energy per site up to order y^{22}. The first few terms are

$$\omega_0/N = -\frac{\mu}{2} - \frac{2y^2}{1+2\mu} - \frac{y^4}{2} + \frac{14y^4}{(1+2\mu)^3}$$
$$+\frac{y^6(-4742-5084\mu-1640\mu^2-368\mu^3-64\mu^4)}{(1+2\mu)^5(3+2\mu)(7+2\mu)}$$
$$+\cdots \tag{53}$$

where ω_0 is the ground-state eigenvalue of W. The coefficients are listed for various fixed values of the dimensionless mass parameter $\mu = 2m/e^2$ in Table III. These coefficients agree with those of reference I up to $O(y^{16})$.

Extrapolating these series into the weak-coupling region using integrated differential approximants [27], one obtains results as shown in Fig. 6. For the large-mass case, $\mu = 10$, it can be seen that the strong-coupling approximants match on to the weak-coupling form (40) very nicely at around $1/y \simeq 0.5$. For the lower masses, the strong-coupling approximants do not converge well enough to establish a precise matching, but they are clearly quite consistent with the asymptotic form (40). It is noteworthy that the

TABLE III. Series coefficients of y^{2n} in strong-coupling expansions of the ground-state energy ω_0 and chiral condensate $\langle\overline{\psi}\psi\rangle^{\text{lattice}}$.

n	$\mu=0$	$\mu=0.5$	$\mu=1$	$\mu=2$	$\mu=10$
			Ground state energy		
0	0.000000000000	$-2.500000000000\times10^{-1}$	$-5.000000000000\times10^{-1}$	-1.000000000000	-5.000000000000
1	-2.000000000000	-1.000000000000	$-6.666666666667\times10^{-1}$	$-4.000000000000\times10^{-1}$	$-9.523809523810\times10^{-2}$
2	$1.350000000000\times10^{1}$	1.250000000000	$1.851851851852\times10^{-2}$	$-3.880000000000\times10^{-1}$	$-4.984882842026\times10^{-1}$
3	$-2.258095238095\times10^{2}$	-7.562500000000	-1.088065843621	$-1.057163636364\times10^{-1}$	$-4.840190310415\times10^{-4}$
4	$4.740493349632\times10^{3}$	$4.168190104167\times10^{1}$	2.828630278758	$1.440413481513\times10^{-1}$	$3.805417269032\times10^{-2}$
5	$-1.145332120404\times10^{5}$	$-2.641393774675\times10^{2}$	-8.251436202716	$-1.196372180167\times10^{-1}$	$7.580050883728\times10^{-5}$
6	$3.019112271993\times10^{6}$	$1.828909211780\times10^{3}$	$2.673208303367\times10^{1}$	$1.528725434873\times10^{-1}$	$-2.829817166242\times10^{-3}$
7	$-8.446045864104\times10^{7}$	$-1.343961734536\times10^{4}$	$-9.195676938217\times10^{1}$	$-2.146264820882\times10^{-1}$	$-8.316158017118\times10^{-6}$
8	$2.467210478469\times10^{9}$	$1.031183072419\times10^{5}$	$3.302984237354\times10^{2}$	$3.075754366619\times10^{-1}$	$-6.084851949294\times10^{-4}$
9	$-7.447992091066\times10^{10}$	$-8.175829204890\times10^{5}$	$-1.226060361259\times10^{3}$	$-4.580923967202\times10^{-1}$	$-3.103254879714\times10^{-6}$
10	$2.307292550322\times10^{12}$	$6.651573204917\times10^{6}$	$4.670066518532\times10^{3}$	$6.989367972569\times10^{-1}$	$4.685274190981\times10^{-4}$
11	$-7.298475917954\times10^{13}$	$-5.525241939727\times10^{7}$	$-1.816217581154\times10^{4}$	-1.087547736352	$2.784016199972\times10^{-6}$
			Chiral condensate		
0	$5.000000000000\times10^{-1}$	$5.000000000000\times10^{-1}$	$5.000000000000\times10^{-1}$	$5.000000000000\times10^{-1}$	$5.000000000000\times10^{-1}$
1	-4.000000000000	-1.000000000000	$-4.444444444444\times10^{-1}$	$-1.600000000000\times10^{-1}$	$-9.070294784581\times10^{-3}$
2	$8.400000000000\times10^{1}$	5.250000000000	1.037037037037	$1.344000000000\times10^{-1}$	$4.319187992657\times10^{-4}$
3	$-2.231056689342\times10^{3}$	$-3.661718750000\times10^{1}$	-3.414650205761	$-1.856045336482\times10^{-1}$	$-1.490233956148\times10^{-4}$
4	$6.534158638592\times10^{4}$	$2.809490017361\times10^{2}$	$1.222412306072\times10^{1}$	$2.632452778514\times10^{-1}$	$1.645776229220\times10^{-5}$
5	$-2.025737847176\times10^{6}$	$-2.284382049423\times10^{3}$	$-4.639999014178\times10^{1}$	$-3.921048572445\times10^{-1}$	$2.005503745248\times10^{-5}$
6	$6.518294767679\times10^{7}$	$1.929013101510\times10^{4}$	$1.831818873072\times10^{2}$	$6.165298249176\times10^{-1}$	$-2.127283455260\times10^{-6}$
7	$-2.153203741629\times10^{9}$	$-1.672676257346\times10^{5}$	$-7.429933326106\times10^{2}$	$-9.978195968035\times10^{-1}$	$-2.070374769933\times10^{-6}$
8	$7.252977297783\times10^{10}$	$1.479158204994\times10^{6}$	$3.074244834593\times10^{3}$	1.648612396832	$1.799802187362\times10^{-7}$
9	$-2.480301602121\times10^{12}$	$-1.327976394916\times10^{7}$	$-1.291627245890\times10^{4}$	-2.768670289809	$-9.300630428741\times10^{-7}$
10	$8.584509655365\times10^{13}$	$1.206675388588\times10^{8}$	$5.492904223987\times10^{4}$	4.708649820309	$1.110110045268\times10^{-7}$
11	$-3.000444314331\times10^{15}$	$-1.107246112597\times10^{9}$	$-2.359089145008\times10^{5}$	-8.090428010991	$7.857720150141\times10^{-7}$

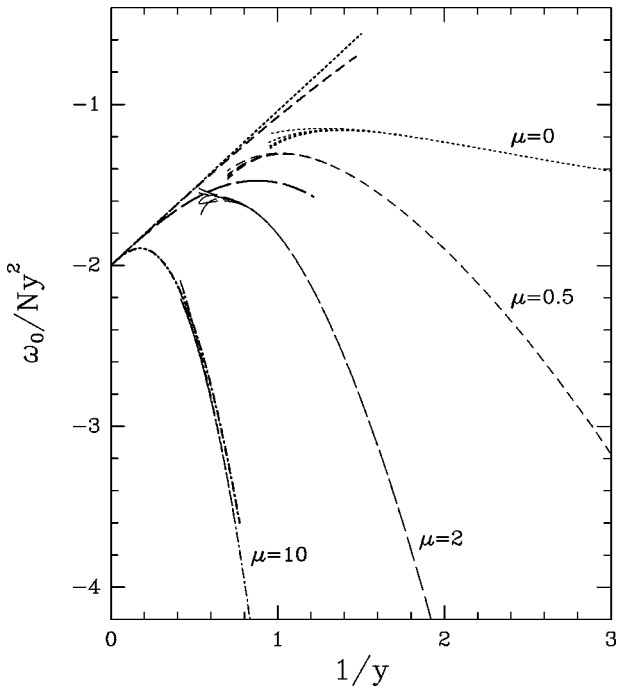

FIG. 6. Graph of the ground-state energy per site, $y^{-2}\omega_0/N$ versus $1/y$, for various fixed values of the mass parameter $\mu=0,0.5,2,10$. The curves at large $1/y$ are integrated differential approximants to the strong-coupling series; while those at small $1/y$ correspond to the asymptotic weak-coupling form (40).

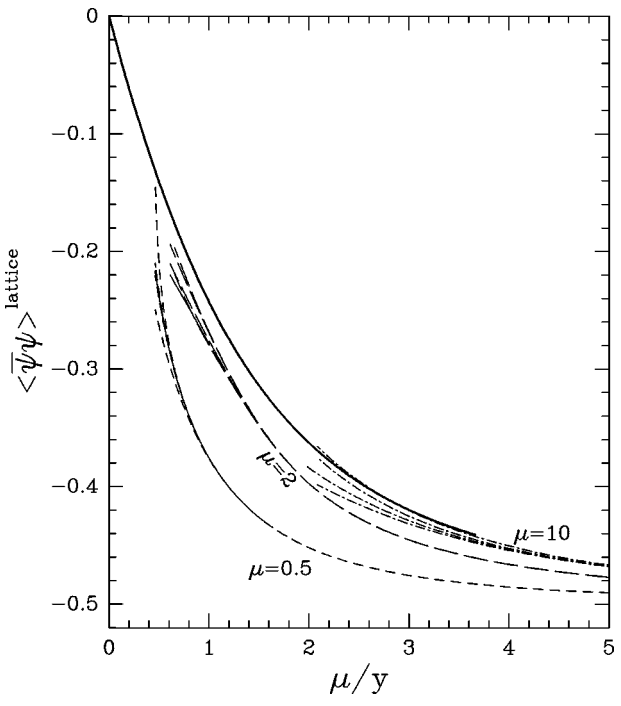

FIG. 7. Graph of the chiral condensate, $\langle\overline{\psi}\psi\rangle^{\text{lattice}}$ versus μ/y, for various finite values of the mass parameter $\mu=0.5,2,10$. The curves at large $1/y$ are various integrated differential approximants and Padé approximants to strong-coupling series, while the solid line at small μ/y is the weak-coupling asymptotic form (42).

μ-independent form (41) is only attained for very weak couplings $\mu^2/y^2 \lesssim 0.4$.

The successful matching between the strong-coupling approximants and the weak-coupling asymptotic form gives some confidence that the series coefficients have been calculated correctly, and that the approximants converge well enough to provide useful information about the weak-coupling (continuum) behavior.

B. Chiral condensate

A more interesting quantity is the chiral condensate. The first few terms in the series are

$$\langle \overline{\psi}\psi \rangle^{\text{lattice}} = -\frac{1}{2} + \frac{4y^2}{1+2\mu} - \frac{84y^4}{(1+2\mu)^4} + \frac{8y^6(122987+245156\mu+181668\mu^2+64656\mu^3+13392\mu^4+2048\mu^5+192\mu^6)}{(1+2\mu)^6(3+2\mu)^2(7+2\mu)^2} + \cdots . \tag{54}$$

Further coefficients at fixed values of μ are listed in Table III. Figure 7 shows the extrapolation of these series into the weak-coupling region, as compared with the weak-coupling form (42). Once again, the large mass results ($\mu = 10$) match very well to the weak-coupling form, while the lower-mass ones have not yet attained it before convergence of the strong-coupling approximants is lost.

The most interesting case is $\mu = 0$, the zero mass limit. A graph of $y^2\langle \overline{\psi}\psi \rangle^{\text{lattice}}$ against $1/y$ is shown in Fig. 8. It can be seen that integrated differential approximants to the series fail to converge below about $1/y \simeq 1.5$, although Padé approximants behave in a more consistent fashion. If taken at face value, the Padé approximants would indicate a very large value of the chiral condensate in the continuum limit $1/y \to 0$,

$$e^{-4}\langle \overline{\psi}\psi \rangle^{\text{physical}} = -0.284(10). \tag{55}$$

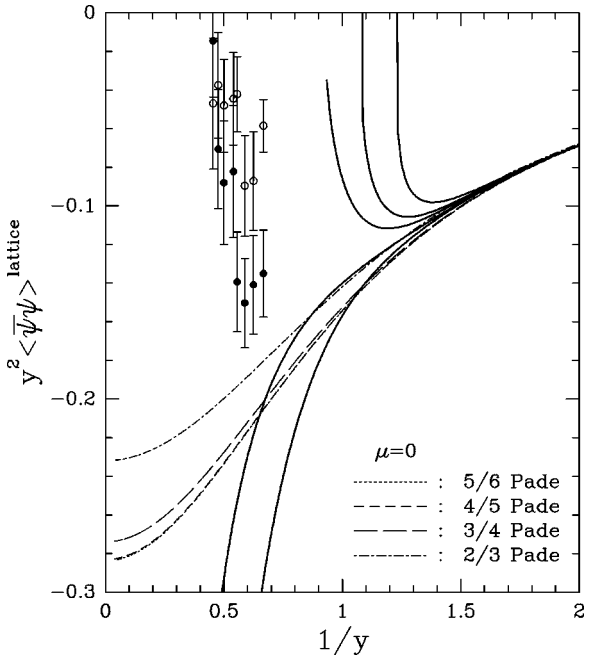

FIG. 8. Graph of the chiral condensate, $y^2\langle \overline{\psi}\psi \rangle^{\text{lattice}}$ versus $1/y$, for the massless case $\mu = 0$. The curves shown are integrated differential approximants (solid lines) and $[n/(n+1)]$ Padé approximants (broken lines) to the strong-coupling series. The last two Padé approximants are almost indistinguishable, and the successive intercepts at $1/y = 0$ are 0.232,0.274,0.283 and 0.284. The data points are from the Euclidean Monte Carlo simulation by Burkitt and Irving [12]: filled points are from quenched approximation, open points for dynamical fermions.

Also shown in Fig. 8, however, are some Monte Carlo estimates of the chiral condensate for the Euclidean version of this model[2] by Burkitt and Irving [12]. Their results are roughly compatible with ours at about $1/y \simeq 0.6$, but show a dramatic decrease in magnitude beyond that point. Since this occurs well below the region of convergence of the series approximants, the series provide little evidence either to confirm or deny this phenomenon.

Another Monte Carlo calculation of the chiral condensate in the noncompact version of the model has been carried out by Dagotto, Kogut and Kocic [7]. They found a quite different behavior, in which $\beta^2\langle \overline{\psi}\psi \rangle^{\text{lattice}}$ (where $\beta = y = 1/g^2$) plunges rapidly toward zero at a low β value around $\beta \simeq 0.4$, and then levels out to a plateau at a very small value, around $\beta^2\langle \overline{\psi}\psi \rangle \simeq 0.001$. Although this value is only tracked to $\beta \simeq 1$, they take this as evidence of chiral symmetry breaking in the continuum limit. A more extensive study by Hands and Kogut [28] revealed substantial finite-size effects, but came to a similar conclusion.

It would be interesting to see a more extensive Monte Carlo simulation of the compact lattice model, to check whether the decrease seen by Burkitt and Irving [12] is real, and whether the chiral condensate subsequently levels out at a small plateau value as in the noncompact model. There seems to be very little prospect that further series calculations could shed light on these questions.

[2]In making this comparison, we assumed the Euclidean coupling g_E and Hamiltonian coupling g_H are equal, lacking information on a more precise connection.

TABLE IV. Series coefficients of y^{2n} in strong-coupling expansions of the symmetric and antisymmetric glueball mass gaps m_S and m_A of the dimensionless Hamiltonian W.

n	$\mu=0$	$\mu=0.5$	$\mu=1$	$\mu=2$	$\mu=10$
			Symmetric glueball mass gaps m_S		
0	4.000000000000	4.000000000000	4.000000000000	4.000000000000	4.000000000000
1	5.333333333333	1.500000000000	-1.066666666667	$-1.523809523810\times10^{-1}$	$-1.743489157677\times10^{-3}$
2	$-4.189814814815\times10^{1}$	-3.135416666667	4.769703703704	$-2.352469495735\times10^{-1}$	$-4.165631870342\times10^{-1}$
3	$5.935307344636\times10^{2}$	$-1.170910493827\times10^{-2}$	$-2.394715197442\times10^{1}$	$-4.890552931893\times10^{-1}$	$-3.937708897154\times10^{-4}$
4	$-3.229319000985\times10^{3}$	$8.663828760713\times10^{1}$	$1.501264118830\times10^{2}$	2.073466005647	$4.945486284578\times10^{-1}$
5	$-6.430232339023\times10^{5}$	$-1.617503042067\times10^{3}$	$-8.784848865979\times10^{2}$	-5.575125327898	$1.071338323552\times10^{-3}$
			Antisymmetric glueball mass gaps m_A		
0	4.000000000000	4.000000000000	4.000000000000	4.000000000000	4.000000000000
1	5.333333333333	1.500000000000	-1.066666666667	$-1.523809523810\times10^{-1}$	$-1.743489157677\times10^{-3}$
2	$-4.306481481481\times10^{1}$	-4.302083333333	3.603037037037	-1.401913616240	-1.583229853701
3	$6.055105324434\times10^{2}$	$1.838348765432\times10^{-2}$	$-2.776504371231\times10^{1}$	$-3.473208512644\times10^{-1}$	$-1.358230163160\times10^{-3}$
4	$9.053923337359\times10^{3}$	$5.354226523059\times10^{1}$	$1.574287286646\times10^{2}$	1.695152914866	1.162208030611
5	$-1.377596830177\times10^{6}$	$-5.970881550866\times10^{2}$	$-9.103588055806\times10^{2}$	$-7.260136671150\times10^{-1}$	$2.449261377761\times10^{-3}$

C. ''Glueball'' masses

Strong-coupling series for the ''photonball'' masses, m_A and m_S, corresponding in the strong-coupling limit to single plaquette excitations which are antisymmetric and symmetric under reflections, respectively, have been calculated to order y^{10}. The leading terms for both series are

$$m_{S,A}=4+16y^2/((1+2\mu)(1-2\mu)(3+2\mu))+O(y^4) \tag{56}$$

with the difference between the two series only emerging at order y^4. Further coefficients at fixed values of μ are listed in Table IV. The coefficients up to $O(y^8)$ were previously calculated in [1].

Approximants to these strong-coupling series are graphed in Figs. 9 and 10, and compared with the results for the pure gauge theory, which we have calculated previously [29] to order y^{32}. It can be seen that for large μ values the series behave very similarly to the pure gauge case, and appear to be decreasing exponentially towards zero as y increases. Our results are consistent with those of Burkitt and Irving [12], who found a systematic downward shift in m_A for moderate quark masses, as seen for the case $\mu=2$ in Figs. 9 and 10. At small μ values, however, the behavior appears to change somewhat. In the region $\mu\lesssim1$, there is substantial overlap and level crossing between the glueball and meson states in

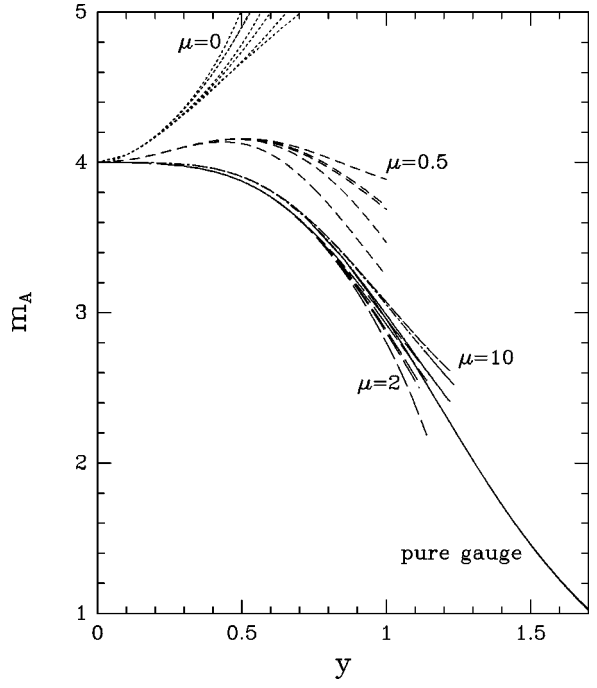

FIG. 9. The mass m_A as a function of y, for $\mu=0,0.5,2,10$, Various integrated differential approximants and Padé approximants to strong-coupling series are shown, together with corresponding results for the ''pure gauge'' case ($\mu=\infty$).

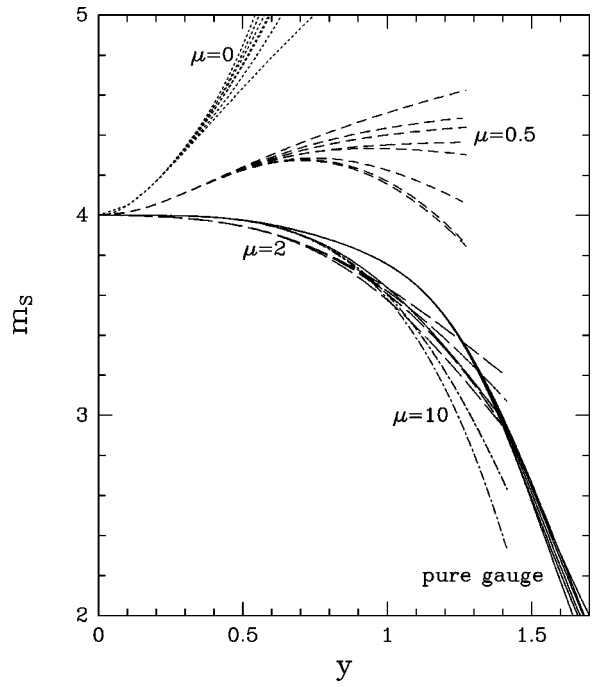

FIG. 10. The mass m_S as a function of y, as in Fig. 9.

the strong-coupling region, and the picture becomes more confused. The series approximants show an initial rise for the glueball masses in the strong-coupling region, followed by an apparent turnover, at least in the $\mu=0.5$ case, but the convergence is not sufficient to track the behavior reliably into the weak-coupling region.

D. Positronium masses

Strong-coupling series for the meson states discussed in Sec. II have been calculated to $O(y^{10})$ [or to $O(y^{12})$ for m_1]. The first three terms for arbitrary μ are

$$m_1=1+2\mu+14y^2/(1+2\mu)-y^4(535+186\mu+60\mu^2+8\mu^3)/[3(1+2\mu)^3]+O(y^6) \tag{57a}$$

$$m_2=m_4=1+2\mu+10y^2/(1+2\mu)-y^4(283+42\mu+12\mu^2+8\mu^3)/[3(1+2\mu)^3]+O(y^6) \tag{57b}$$

$$m_3=1+2\mu+6y^2/(1+2\mu)+y^4(-175+6\mu+36\mu^2-8\mu^3)/[3(1+2\mu)^3]+O(y^6) \tag{57c}$$

$$m_5=m_6=1+2\mu+6y^2/(1+2\mu)-y^4(199+66\mu+12\mu^2+8\mu^3)/[3(1+2\mu)^3]+O(y^6) \tag{57d}$$

$$m_7=m_8=1+2\mu+6y^2/(1+2\mu)-y^4(199+66\mu+12\mu^2+8\mu^3)/[3(1+2\mu)^3]+O(y^6). \tag{57e}$$

Further terms at selected values of μ are given in Table V.

Figure 11 graphs the various meson masses as functions of $1/y$, at a fixed, large mass parameter $\mu=10$. It can be seen that the series approximants for these masses do not converge below about $1/y\simeq 1.5$. For the lowest vector meson states there is a suggestion that the mass reaches a peak at $1/y\simeq 1.5$, and then turns downward. A crude linear extrapolation has been made to estimate the continuum limit, but the uncertainly in the estimate is large.

The resulting values for the vector mass are graphed as a function of μ in Fig. 12, along with the Schwinger-Dyson estimates of Allen and Burden [15], and the nonrelativistic prediction [19–21]. It can be seen that the lattice estimates of the positronium binding energy have large errors, especially at smaller μ, and lie about three times higher than the Schwinger-Dyson values. Neither the Schwinger-Dyson nor the lattice estimates show any definite evidence of the logarithmic increase at large μ predicted by the nonrelativistic theory.

Figure 13 shows the masses as functions of $1/y$ for the massless case $\mu=0$. Once again, convergence is lost at rather small y values, around $1/y\simeq 2.5$, and it is hardly possible to make useful estimates of the continuum limit. There is no sign of any of the masses dropping towards zero, or acting like a Goldstone boson. This is because the expected Goldstone boson states are the ''axiscalar'' and ''axipseudoscalar'' states [15], which are not among the single-link excitations in the strong-coupling limit which we have treated here (see Sec. II D). The Goldstone bosons probably correspond to L-shaped double-link excitations, which will transform into each other under a single plaquette excitation. It would be interesting to study their behavior, but we have not yet attempted such a study, owing to technical complications.

V. SUMMARY AND DISCUSSION

New strong-coupling series have been presented for the ground-state energy and chiral condensate, along with the ''glueball'' and positronium masses, in 4-component Hamiltonian lattice QED_{2+1} with full dynamical fermions. This represents the first attempt at a series calculation for the positronium states in this model.

Two major features are evident from these results. Firstly, there is a very clear separation of scales between the ''glueballs'' and the positronium states as the continuum limit is approached. At large fermion mass μ, the positronium energies remain finite in the continuum limit, while the ''glueball'' masses scale exponentially towards zero, presumably corresponding in the limit to massless photon states. The same thing appears to happen at smaller μ values, although our evidence for the exponential decrease of the glueball mass is rather slim. This separation of scales is consistent with earlier discussions of the pure gauge model [30]: in the nonrelativistic or static fermion limit, if one sticks to naive ''engineering'' dimension scales one will end up with a theory of free, massless photons as above, whereas if one renormalizes the scale as discussed by Polyakov [31] or Göpfert and Mack [32] one will obtain a theory of free, *massive* bosons.

The second feature is that the addition of dynamical fermions does not greatly affect the glueball masses at large μ: at $\mu=2$, for instance, the only effect was a reduction of the

TABLE V. Series coefficients of y^{2n} in strong-coupling expansions of the meson mass gaps m_i ($i=1,2,\ldots,8$) of the dimensionless Hamiltonian W.

n	m_1	$m_2=m_4$	m_3	$m_5=m_6$	$m_7=m_8$
			$\mu=0$		
0	1.000000000000	1.000000000000	1.000000000000	1.000000000000	1.000000000000
1	$1.400000000000\times10^{1}$	$1.000000000000\times10^{1}$	6.000000000000	6.000000000000	6.000000000000
2	$-1.783333333333\times10^{2}$	$-9.433333333333\times10^{1}$	$-5.833333333333\times10^{1}$	$-6.633333333333\times10^{1}$	$-6.633333333333\times10^{1}$
3	$3.625151675485\times10^{3}$	$1.757293650794\times10^{3}$	$1.200151675485\times10^{3}$	$1.341849206349\times10^{3}$	$1.253207231041\times10^{3}$
4	$-9.101099254509\times10^{4}$	$-4.164808339711\times10^{4}$	$-2.976672075609\times10^{4}$	$-3.324256060799\times10^{4}$	$-3.008509651089\times10^{4}$
5	$2.534993350264\times10^{6}$	$1.113036398112\times10^{6}$	$8.177458288471\times10^{5}$	$9.143840136437\times10^{5}$	$8.115398963424\times10^{5}$
6	$-7.521807853058\times10^{7}$				
			$\mu=0.5$		
0	2.000000000000	2.000000000000	2.000000000000	2.000000000000	2.000000000000
1	7.000000000000	5.000000000000	3.000000000000	3.000000000000	3.000000000000
2	$-2.683333333333\times10^{1}$	$-1.283333333333\times10^{1}$	-6.833333333333	-9.833333333333	-9.833333333333
3	$1.365322916667\times10^{2}$	$6.154340277778\times10^{1}$	$4.075451388889\times10^{1}$	$5.498784722222\times10^{1}$	$4.683784722222\times10^{1}$
4	$-8.920838363922\times10^{2}$	$-3.876159660218\times10^{2}$	$-2.760344845403\times10^{2}$	$-3.678279451885\times10^{2}$	$-2.870075748181\times10^{2}$
5	$6.436060668280\times10^{3}$	$2.730071323411\times10^{3}$	$2.011538052494\times10^{3}$	$2.664691694041\times10^{3}$	$2.110416878518\times10^{3}$
6	$-4.984333949987\times10^{4}$				
			$\mu=1$		
0	3.000000000000	3.000000000000	3.000000000000	3.000000000000	3.000000000000
1	4.666666666667	3.333333333333	2.000000000000	2.000000000000	2.000000000000
2	-9.740740740741	-4.259259259259	-1.740740740741	-3.518518518519	-3.518518518519
3	$2.117987280210\times10^{1}$	9.052263374486	5.541189674523	9.760905349794	6.595922184811
4	$-7.103051896801\times10^{1}$	$-2.746737478771\times10^{1}$	$-1.941553551960\times10^{1}$	$-3.281454899895\times10^{1}$	$-2.157173735275\times10^{1}$
5	$2.054506982964\times10^{2}$	$9.091443816105\times10^{1}$	$6.590006451270\times10^{1}$	$1.138794166995\times10^{2}$	$7.209915733050\times10^{1}$
6	$-8.384073194275\times10^{2}$				
			$\mu=2$		
0	5.000000000000	5.000000000000	5.000000000000	5.000000000000	5.000000000000
1	2.800000000000	2.000000000000	1.200000000000	1.200000000000	1.200000000000
2	-3.229333333333	-1.277333333333	$-2.213333333333\times10^{-1}$	-1.181333333333	-1.181333333333
3	3.119580472860	$8.464108513709\times10^{-1}$	$4.398750760351\times10^{-1}$	1.428440057720	$9.870369807970\times10^{-1}$
4	-4.249661491769	-1.098495894429	$-8.941846899782\times10^{-1}$	-2.414224882476	-1.183255224582
5	9.281773558871	1.580697986782	1.236101545345	4.024451851449	2.130785627667
6	$-2.667077094545\times10^{1}$				
			$\mu=10$		
0	$2.100000000000\times10^{1}$	$2.100000000000\times10^{1}$	$2.100000000000\times10^{1}$	$2.100000000000\times10^{1}$	$2.100000000000\times10^{1}$
1	$6.666666666667\times10^{-1}$	$4.761904761905\times10^{-1}$	$2.857142857143\times10^{-1}$	$2.857142857143\times10^{-1}$	$2.857142857143\times10^{-1}$
2	$-5.901090594968\times10^{-1}$	$-3.564409890941\times10^{-1}$	$-1.625094482237\times10^{-1}$	$-3.620559334845\times10^{-1}$	$-3.620559334845\times10^{-1}$
3	$-2.582504019689\times10^{-3}$	$-1.053385459541\times10^{-2}$	$1.090172643379\times10^{-2}$	$3.819111465784\times10^{-2}$	$1.199822627856\times10^{-2}$
4	$2.457235107452\times10^{-1}$	$1.646791697513\times10^{-1}$	$7.346442898971\times10^{-2}$	$1.373283015502\times10^{-1}$	$1.747678732566\times10^{-1}$
5	$6.900777782581\times10^{-2}$	$1.213278624644\times10^{-2}$	$-7.752772094654\times10^{-3}$	$5.188958501563\times10^{-3}$	$-8.047408934744\times10^{-3}$
6	$-1.752056769026\times10^{-1}$				

glueball mass at fixed y of order a percent or two. For $\mu \lesssim 0.5$ the effect is more pronounced, however.

In general, the results of these calculations were somewhat disappointing. The bulk ground-state energy per site converged well enough into the weak-coupling region to display a convincing match with analytic weak-coupling expansions [16], and the ''glueball'' masses converged well enough to justify the statements given above. Other quantities, however, were not mapped out with such success. Series approximants to the chiral condensate at $\mu=0$ only converged down to $1/y\simeq1.5$, and were unable to confirm or deny the rapid plunge in magnitude seen by Burkitt and Irving [12] around $1/y\simeq0.5$. It will require more detailed Monte Carlo studies to confirm that this plunge really occurs, and to determine whether the chiral condensate then levels out at a small but finite value.

Series approximants to the positronium masses likewise only converged down to $1/y\simeq1.5$, even at large mass μ, making any extrapolations to the continuum limit very uncertain. Our estimates of the continuum ''binding energy''

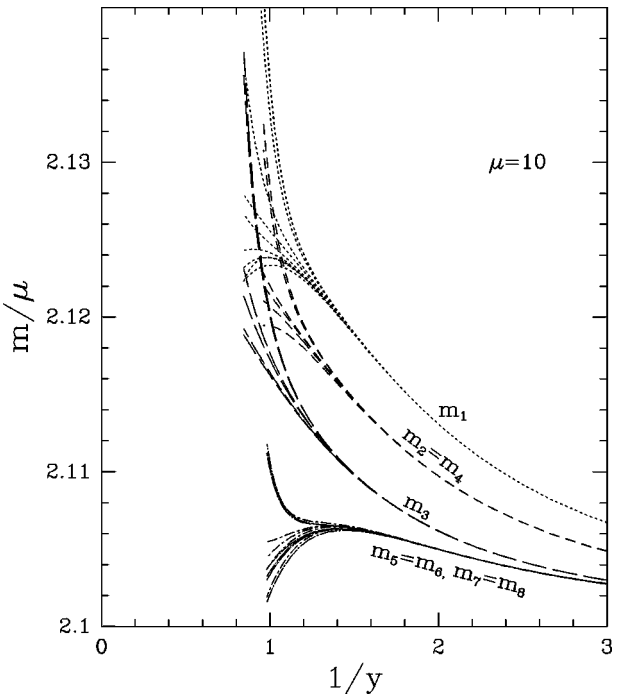

FIG. 11. Strong-coupling series approximants to m/μ as functions of $1/y$ for the meson states $m_1, \ldots, m_8$, at mass parameter $\mu = 10$.

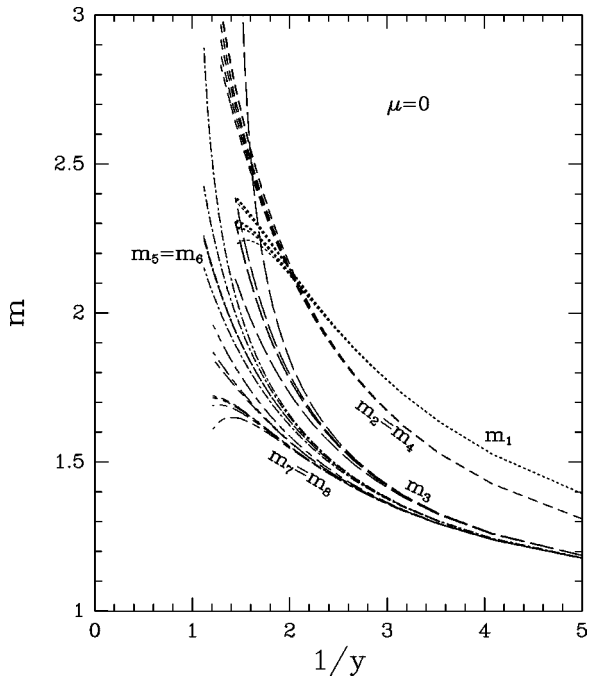

FIG. 13. Series approximants to $m_1, \ldots, m_8$ versus $1/y$ at $\mu = 0$.

are thus of little more than qualitative accuracy. They lie about three times higher than the Schwinger-Dyson estimates of Allen and Burden [15], which are not expected to be very accurate at large mass μ in any case. Neither set of results shows any definite sign of the logarithmic increase in energy with μ predicted by the nonrelativistic analyses [19–21]. Once again, a detailed understanding of the positronium spectrum must await a more accurate study, by Monte Carlo or other methods.

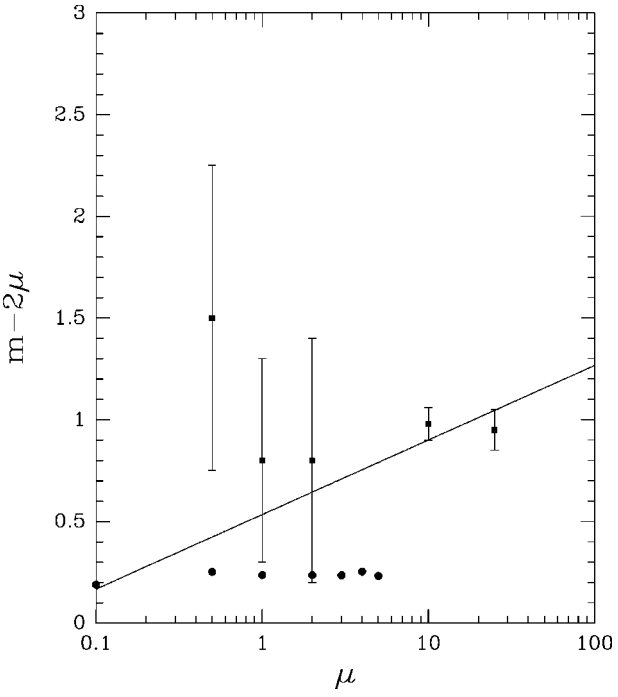

FIG. 12. Graph of m/μ versus μ for the vector state m_7.

The question whether this model develops Goldstone bosons in the massless limit $\mu = 0$ was not explored. These ''axiscalar'' and ''axipseudoscalar'' states [15] are not among the single-link excitations for which we have calculated strong-coupling expansions. They are most likely to be found among the ''double-link'' excitations. It is technically more difficult to calculate strong-coupling series for the double-link excitations; but on the other hand, the series may well converge more quickly for these low-lying excitations. This might provide an interesting subject for further study.

In general, however, the prospects for further series calculations look dim. In contrast to the Schwinger model case [23], the strong-coupling series approximants do not converge far enough into the weak-coupling region to allow accurate extrapolations to the continuum limit. Thus it seems there is still no real alternative to Monte Carlo methods, whatever their limitations, for the detailed investigation of lattice gauge theories in three and four dimensions. The strong-coupling series provide an accurate ''platform'' of results in the strong-coupling region, which can provide useful calibration points for other methods; but their extrapolation into the weak-coupling region remains rather uncertain. There is a possibility, however, that the use of an ''improved Hamiltonian'' [33] could improve the situation here.

ACKNOWLEDGMENTS

We are very grateful for helpful comments from Conrad Burden and Alan Irving. This work forms part of a research project supported by a grant from the Australian Research Council.

[1] J. M. Cornwall, Phys. Rev. D **22**, 1452 (1980).
[2] R. D. Pisarski, Phys. Rev. D **29**, 2423 (1984); T. W. Appelquist, M. Bowick, D. Karabali, and L .C. R. Wijewardhana, Phys. Rev. Lett. **55**, 1715 (1985); Phys. Rev. D **33**, 3704 (1986).
[3] G. Baskaran and P. W. Anderson, Phys. Rev. B **37**, 580 (1988); I. Affleck and J. Marston, *ibid.* **37**, 3774 (1988); E. Dagotto, E. Fradkin, and A. Moreo, *ibid.* **38**, 2926 (1988).
[4] S. Deser, R. Jackiw, and S. Templeton, Ann. Phys. (N.Y.) **140**, 372 (1982); J. F. Schonfeld, Nucl. Phys. **B185**, 157 (1981); A. J. Niemi and G. W. Semenoff, Phys. Rev. Lett. **51**, 2077 (1983); A. N. Redlich, Phys. Rev. D **29**, 2366 (1984).
[5] C. J. Burden and A. N. Burkitt, Europhys. Lett. **3**, 545 (1987).
[6] M. R. Pennington and D. Walsh, Phys. Lett. B **253**, 246 (1991); D. C. Curtis, M. R. Pennington, and D. Walsh, *ibid.* **295**, 313 (1992).
[7] E. Dagotto, J. B. Kogut, and A. Kocic, Phys. Rev. Lett. **62**, 1083 (1989); Nucl. Phys. **B334**, 279 (1990).
[8] T. Appelquist, D. Nash, and L. Wijewardhana, Phys. Rev. Lett. **60**, 2575 (1988); D. Nash, *ibid.* **62**, 3024 (1989).
[9] V. P. Gusynin, A. H. Hams, and M. Reenders, Phys. Rev. D **53**, 2227 (1996).
[10] P. Maris, Phys. Rev. D **54**, 4049 (1996).
[11] K. Farakos and G. Koutsoumbas, Phys. Lett. B **178**, 260 (1986).
[12] A. N. Burkitt and A. C. Irving, Nucl. Phys. **B295**, 525 (1988).
[13] C. J. Burden, Nucl. Phys. **B387**, 419 (1992); P. Maris, Phys. Rev. D **52**, 6087 (1995).
[14] C. J. Burden and C. D. Roberts, Phys. Rev. D **44**, 540 (1991).
[15] T. W. Allen and C. J. Burden, Phys. Rev. D **53**, 5842 (1996); **55**, 4954 (1997).
[16] C. J. Burden and C. J. Hamer, Phys. Rev. D **37**, 479 (1988).
[17] J. M. Aroca and H. Fort, Phys. Lett. B **317**, 604 (1993).
[18] M. Burkardt and A. Langnau, Phys. Rev. D **44**, 1187 (1991).
[19] A. Tam, C. J. Hamer, and C. M. Yung, J. Phys. G **21**, 1463 (1995).
[20] J. M. Cornwall and G. Tiktopoulos, Phys. Rev. D **15**, 2937 (1977); D. Sen, *ibid.* **41**, 1227 (1990).
[21] C. M. Yung and C. J. Hamer, Phys. Rev. D **44**, 2595 (1991); V. G. Koures, J. Comput. Phys. **128**, 1 (1996).
[22] For a review, see H. X. He, C. J. Hamer, and J. Oitmaa, J. Phys. A **23**, 1775 (1990).
[23] C. J. Hamer, W. H. Zheng, and J. Oitmaa, Phys. Rev. D **56**, 55 (1997).
[24] L. Susskind, Phys. Rev. D **16**, 3031 (1977).
[25] J. Kogut and L. Susskind, Phys. Rev. D **11**, 395 (1975).
[26] M. F. L. Golterman, Nucl. Phys. **B273**, 663 (1986).
[27] For a review, see A.J. Guttmann, in *Phase Transitions and Critical Phenomena*, edited by C. Domb and J.L. Lebowitz (Academic, New York, 1989), Vol. 13.
[28] S. Hands and J. B. Kogut, Nucl. Phys. **B335**, 455 (1990).
[29] C. J. Hamer, W. H. Zheng, and J. Oitmaa, Phys. Rev. D **45**, 4652 (1992).
[30] L. Gross, Commun. Math. Phys. **92**, 137 (1983); C. J. Hamer and W. H. Zheng, Phys. Rev. D **48**, 4435 (1993).
[31] A. M. Polyakov, Phys. Lett. **59B**, 82 (1975).
[32] M. Göpfert and G. Mack, Commun. Math. Phys. **82**, 545 (1982).
[33] G. P. Lepage and P. B. Mackenzie, Phys. Rev. D **48**, 2250 (1993).